Laser-Induced Breakdown Spectroscopy (LIBS) analysis of laser processing in active crystal with nanosecond laser pulses

Fernando C. Alvira,* Airan Ródenas, Gustavo A. Torchia

Centro de Investigaciones Ópticas CIC-Conicet La Plata, Casilla de Correos 3 La Plata (1897) Argentina

Laser-induced breakdown spectroscopy (LIBS) analysis is applied to study the ablation threshold and the main plasma features of active crystals used for laser processing with Nd^{3+} ions. The experiments were conducted by using nanosecond laser pulses from a neodymium-doped yttrium aluminum garnet laser and its harmonics. In particular, we have studied the ablation process in SBN, strontium barium niobate ($Sr_xBa_{1-x}Nb_2O_6$, $x = 0.6$), and SBN, sodium barium niobate ($Ba_2NaNb_5O_{15}$), nonlinear and ferroelectric crystals. Two different ablation regimes have been identified by LIBS analysis with high sensitivity compared with the standard method of hole-diameter measurement. Analyzing spectroscopically the plasma emission, we have found a particular behavior with the excitation wavelength. For example, the electronic density and temperature in SBN-generated plasmas present an abnormal behavior with the excitation wavelength. We therefore conclude that the energy gap corresponding to these crystals plays an important role in describing this fact. Hence, the resonant ablation in doped crystals can be a suitable point for exploration in further works in order to use the plasma performances to optimize the laser processing by nanosecond pulses for technological applications.

Index Headings: **Laser-induced breakdown spectroscopy; LIBS; Laser crystals; Sodium barium niobate; BNN; Strontium barium niobate; SBN.**

Introduction

Laser processing of materials applied for tailored integrated optical circuits has recently been an important procedure used for the fabrication of photonics devices. Online and real-time diagnosis of the tailoring process is a requirement of this kind of laser processing. As an example, when a ridge waveguide is defined on a thin film deposited over the substrate, the laser ablation threshold (LAT) and qualitative composition of the material under excitation should be known. The LAT is important because it enables us to know if the laser is interacting with the thin film or with the substrate. One condition that must be fulfilled is that the LAT of the substrate must be greater than the thin film to ensure a complete remotion in the interaction zone. In addition, the qualitative composition of the material can be known by spectroscopically analyzing the plasma formed due to the laser-matter interaction. This analysis tells us if the laser is interacting only with the thin film (the desired condition) or with the substrate.

Received 2 May 2013; accepted 26 November 2013.
* Author to whom correspondence should be sent. E-mail: fcalvira@ciop.unlp.edu.ar.
DOI: 10.1366/13-07072

We use laser-induced breakdown spectroscopy (LIBS) to determine both the elemental composition of the sample and the LAT. Laser-induced breakdown spectroscopy is a well-known spectroscopic technique whose main characteristics are that it needs no sample preparation and offers reduced analysis time, portability, and usefulness for online analysis.[1–9] Not much work has been done using LIBS as an analytical technique for laser crystals characterization.[10] Thus, there are still many unanswered questions regarding the fundamental mechanisms underlying the nanosecond laser interaction with crystals. Gordillo-Vázquez et al.[10] made a plasma characterization of lithium fluoride (an optical crystal) in vacuum conditions. However, they did not fully characterize the ablation process, i.e., they did not estimate a key parameter for laser processing such as the ablation threshold. Therefore, in order to control and optimize the micromodified regions made with nanosecond pulses, laser-matter interaction dynamics need to be further explored. Laser-induced breakdown spectroscopy could be a simple and efficient tool to reach these goals.[11,12]

The laser ablation threshold (LAT) is an important parameter that must be known before beginning the laser processing. Proofs of this fact are the many methods developed to measure the LAT. One of the first methods used is based on photothermal deflection, by detecting the refractive index gradient changes around the crater formed by the ablation process.[13–15] Another widely used procedure is the measurement of the diameter or depth of the craters produced, assuming a Gaussian beam profile for the laser.[16,17] There are also methods based on the measurement of the quantity of mass extracted[18] and procedures that use a high-speed framing camera to photograph the movement of the material ejected from the surface.[19] The measurement of photo-induced electricity and the charge of ionized species stemming from the ablation process have also been reported for the determination of LAT.[20] Laser ablation induced photo-acoustics (LAIP) was also used to determine the LAT in a nanosecond ablation regime.[5,21,22] Using this technique, it has been shown that acoustic detection with a microphone makes it possible to monitor the ablation process in real time and performs ablation curves in a simpler and cheaper way. Laser plasma emission (without spectral resolution) has been used to measure the ablation threshold of steel plates,[23] and the light emission was compared with the acoustical signal emitted during the ablation. On the other hand, the ablation threshold of ancient glass has been measured

0003-7028/14/6804-000000/0

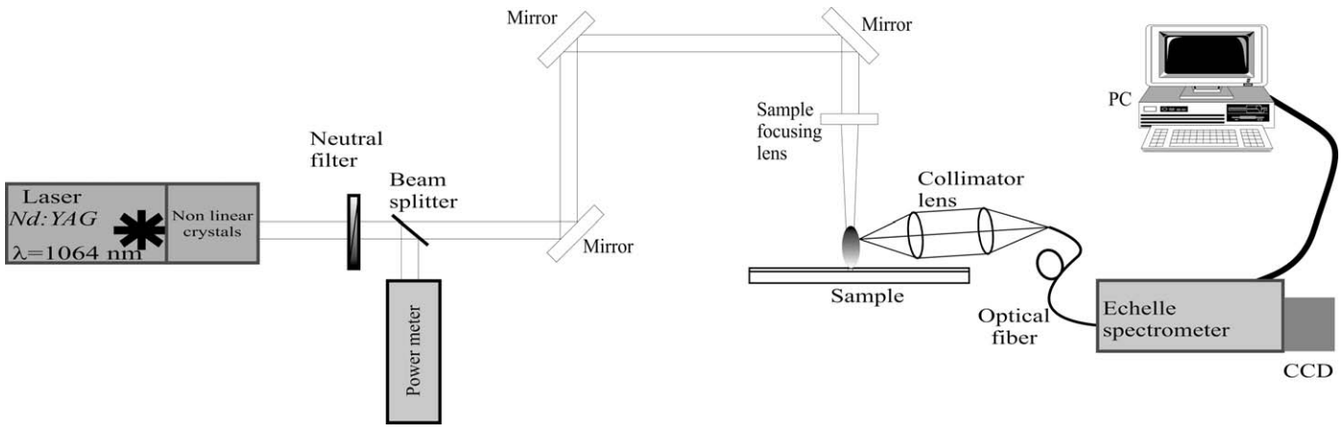

FIG. 1. Experimental setup used to carry out the nanosecond laser ablation in laser crystals.

by using the emission of Si atoms from the ablation plasma.[24]

Usually, ultraviolet (UV) nanosecond pulsed lasers are the main radiation source used in the micromachining of optical circuits.[25–28] In recent years, ultra-short laser writing for high and low repetition rates has emerged as a robust technique, mainly due to the drastic reduction of thermal effects during the laser-assisted procedure.[29–31] Nowadays, the fabrication of two-dimensional (2D) and three-dimensional (3D) microstructures by direct laser writing is an active field of research, demanding a strong knowledge of laser-matter interaction. This fact is evident from the growing requirements for compact and efficient production of photonic applications. The main advantages of laser ablation are outstanding spatial resolution, low sample contamination, and fast processing speed. Nevertheless, the possible existence and nature of permanent microstructural modifications induced during the laser-writing process is still an open question. Therefore, attention should be focused on studying the optical properties around the tracks defined by the laser-writing procedure. Optical microscopy as well as high-sensitivity techniques such as microluminescence, micro-Raman, and scanning near-field optical microscopy (SNOM) has been successfully used to test the optical properties of the treated crystals.[32–34]

Strontium barium niobate (SBN) and sodium barium niobate (BNN) are currently being studied due to their high electro-optical and nonlinear optical coefficients for photonic applications. These crystals are ferroelectrics in which microdomain engineering is possible, and is of great relevance for the development of second-order photonic structures.[35–37] Additionally, these samples have the advantage of being easily doped with rare earth elements, becoming a crystal laser host. Suitable laser action of Nd^{3+}-doped SBN and BNN crystals has been reported.[36,38]

The aim of this work is to characterize by using LIBS the laser-matter interaction for optical materials employed in laser processing, particularly studying Nd^{3+}-doped BNN and SBN crystals. Different ablation regimes in nanosecond ablation are experimentally identified and discussed. By using LIBS, the ablation threshold for each regime was measured and compared with a standard method. Also, by using spectroscopic data, we have determined plasma temperature and electron density as a function of the incident wavelength to get a better understanding of laser-matter interaction in photonics materials. Finally, to assess the importance of the matrix effect in the laser-writing process, we have studied and discussed it.

Experimental procedure

Figure 1 sketches the experimental setup used to perform the experiments. The samples were mounted in an XYZ motorized station perpendicular to the direction of laser incidence. A 100 mm lens was used to focus the laser onto the sample. The plasma emission was analyzed employing a set of two lenses, to collimate and focus the light into a fiber (0.1 mm opening) attached to a cross-dispersion Echelle spectrometer (Mechelle Multichannel Instruments) with a charge-coupled device (CCD) incorporated camera of 280 × 1024 pixels. This spectroscopic setup enables simultaneous detection of a large spectral region and range (350 to 1100 nm with a 0.3 nm spectral resolution) in a single laser shot. The spectral response of this system is corrected internally by software by manufacturer. This correction is done in such a way that the answer is nearly a plateau in all the spectral range of the instrument.

The ablation process was carried out by means of a Nd : YAG nanosecond pulsed laser from Continuum Company (USA), delivering 10 ns pulses width, 10 Hz repetition rate, and up to 400 mJ of energy per pulse. Experiments at 532 and 355 nm were done by using a second- and third-harmonic generation system. The energy delivered by the laser was measured by a thermopile, and it was controlled by using neutral density filters.

Determination of the ablation threshold in these LIBS experiments was done by employing two consecutive laser pulses. The first of the pulses is used to clean the surface, and the second one is intended to acquire the Ba II ($\lambda = 455.41$ nm) emission line intensity. If the emission of the first laser pulse only is taken, then the measured parameter would be the ablation threshold of the dirt deposited over the samples, as is demonstrated by Orzi et al.[23]

Strontium barium niobate ($Sr_xBa_{1-x}Nb_2O_6$, $x = 0.6$) and BNN ($Ba_2NaNb_5O_{15}$) crystals doped with Nd^{3+} were cut in slabs with dimensions of $2 \times 5 \times 5$ mm with surfaces polished up to optical grade by using diamond powder with the lowest size of 0.25 μm. The Nd^{3+} concentration was 1% for every crystal.

The absorption spectra were measured using a Beckman DU-65 UV-visible spectrophotometer under room temperature conditions.

Results and discussions

Ablation threshold determination. As shown in Fig. 2, emission lines from all the constitutive atoms of BNN samples, namely Ba, Nb, O, and Na, were obtained. In the case of Ba, we identified the emission of the neutral and single ionized species. The spectra shown in Figs. 2d, 2e, and 2f correspond to the emitting elements present in the ablation plume obtained for SBN crystals, excited at 1064, 532, and 355 nm, respectively. As can be seen, the emission spectra of all the elements in the samples were found (Sr, Ba, Nb, O, and Nd).

In order to characterize the ablation regimes for the Nd^{3+}-doped crystals used in these experiments, we carried out two different experimental methods. The physical meaning of those regimes is a change in the ablation rate. In the so-called region II, the quantity of material extracted by each laser pulse is larger than in region I. The ablation threshold is measured by extrapolating with a linear regression the region II until the *x*-axis is intercepted. By contrast, region I is related to the damaged threshold, which is always less than the ablation threshold. Therefore, the ablation and damage thresholds are different parameters. While the ablation threshold is related with the minimum fluence needed to extract material, the damage threshold can be produced with no material extraction.

We conducted a standard method by measuring the diameter (D) of the ablation holes as a function of the fluence impinging on the sample. To determine the size of the ablated hole, we explored the crater topography, after the ablation process at 355 nm, by using an optical microscopy. To describe this, we included optical microscope pictures (see Figs. 3a and 3b) corresponding to the ablation spots made during the experiments for both samples. As can be seen, the diameter for both holes is the same, about 30 μm, and the spot shows an almost circular shape.

Figure 3c shows the D^2 versus ablation fluence (for data representation, the ordinate axis was set in log scale), and as can be seen, the open and full circles correspond to the Nd : BNN and Nd:SBN crystals, respectively. In these experiments, we tested the diameter of the holes, after irradiation with five laser pulses at 355 nm wavelength, as a function of the pulse fluence. From this figure, we can see complex behavior for every curve. Only for the SBN crystal, we determined from the experimental data the ablation threshold equal to 1.7 ± 0.2 J/cm^2, while region I intersects the axis of fluence at a value of 0.6 ± 0.2 J/cm^2 (see Fig. 3c). This second region is related with a change in the ablation rate. In contrast, for the case of the BNN, the relationship between D^2 versus the fluence presents strange behavior, and drawing conclusions is not a straightforward task.

In the second experiment carried out, we used the LIBS technique to build the ablation curve, which means the emitted intensity (for a given atomic and ionic line) against the incident fluence. We analyzed the emission coming from Ba II (455.41 nm) present in the ablation plume after two laser pulses at 355 nm. Figure 4a shows the emission line intensity versus the fluence in linear scale. The ablation regime for lower fluences (region I) presents a flat dependence. On the other hand, from this figure, as can be seen, the ablation threshold in region II, reached at higher fluences, can be easily determined by fitting the experimental points by a linear curve. Thus, we obtained ablation threshold values for the two crystals as 2.1 ± 0.2 and 1.9 ± 0.2 J/cm^2 corresponding to Nd : SBN and Nd : BNN, respectively.

To explore both regions in detail, we constructed the same curve in a log-log scale. Figure 4b shows these data. By fitting the experimental values, we can obtain ablation thresholds of 2.1 ± 0.4 and 1.92 ± 0.3 J/cm^2 for the Nd : SBN and Nd : BNN crystal, respectively. On the other hand, both ablation regimes can be explained taking into account the post-breakdown model as it is described by Radziemsky et al.[39] The lower fluence regime (region I) matches the laser-supported combustion model (up to 0.2 J/cm^2 and plasma temperatures lower than 30 000 K), while for region II, fluence values ranged from 0.1 to 20 J/cm^2 and plasma temperatures greater than 30 000 K corresponds to the laser-supported detonation model. A detailed description of those post-breakdown models is given in chapter 2 of Radziemsky et al.[39]

The two different ablation regimes discussed above are in agreement with the theoretical model presented in the literature (Radziemsky et al.[39]). We think that it may be possible to observe this due to the higher sensitivity of the LIBS technique compared with standard methods used for ablation threshold determination. We propose this method as a suitable and sensitive procedure for ablation threshold determination.

Matrix effect. As is well known, LIBS has some deficiencies giving quantitative information. Several papers have tried to explain this drawback, arguing that the matrix effect could be a possible explanation. In brief, the matrix effect can be understood in terms of the responsiveness of the emission of the species. This means that an element at the same concentration level in two different environments (different matrices) can show different atomic and ionic relative intensities and, therefore, that the emission intensity does not follow the sample stoichiometry. This fact has been explained in recent papers and books, taking into account several processes such as the selective ablation, cohesive forces, and sublimation phases, among others.[2,39–41]

With this fact in mind, we observed for the three excitation wavelengths employed (1064, 532, and 355 nm) a discrete contribution of the Nd^{3+} intensity emission for the SBN. By contrast, the situation is different in the BNN case. The BNN sample (see Fig. 2) shows a clear dependence on the excitation wavelength of the Nd emission lines. This means that, when BNN is excited at 532 nm, the emission intensity of Nd ions is clearly greater than in the other two cases. This effect is not

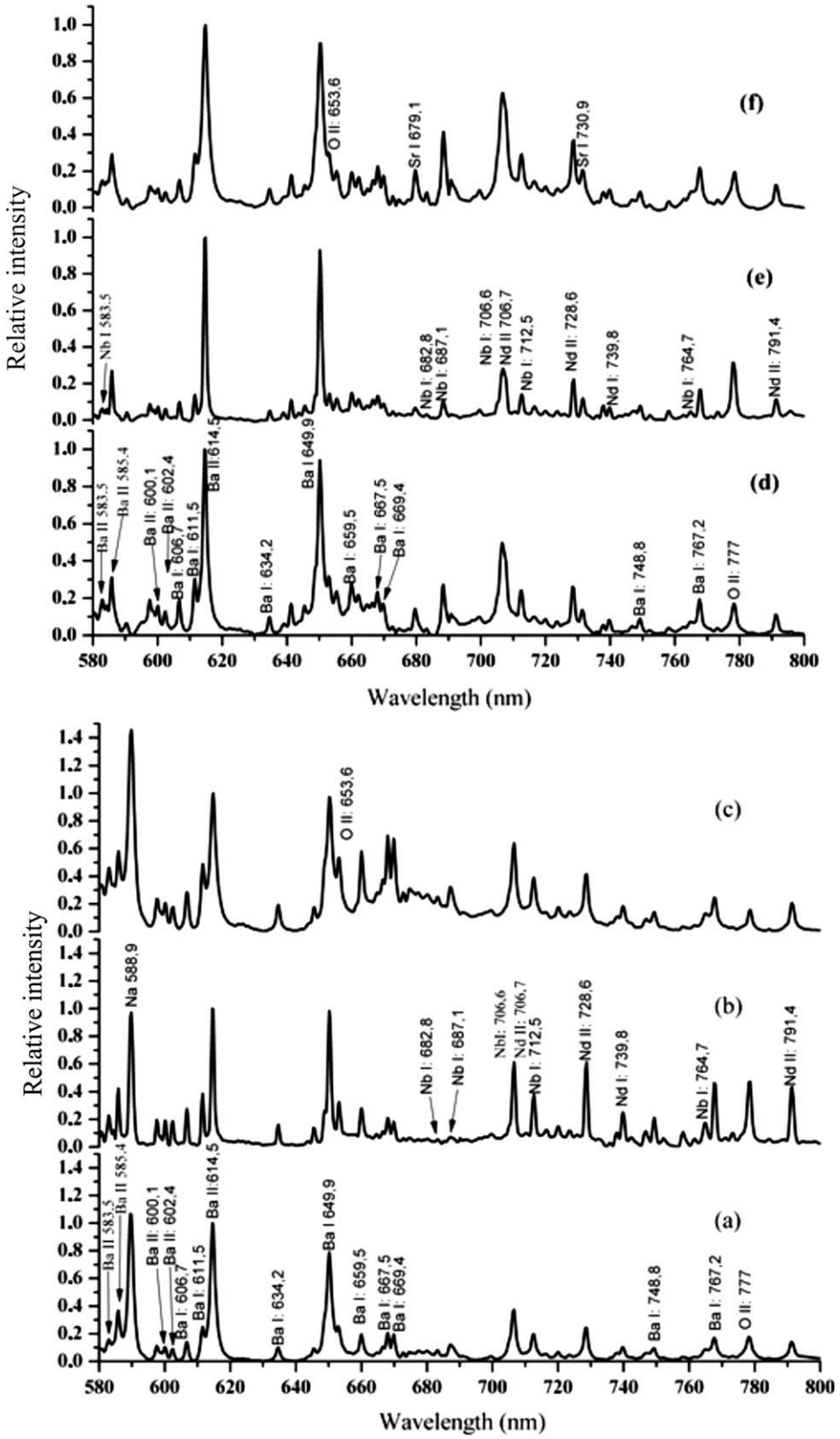

FIG. 2. LIBS spectra (***a***) and (***d***) 1064 nm, (***b***) and (***e***) 532 nm, and (***c***) and (***f***) 355 nm, corresponding to (**a**)–(**c**) BNN and (**d**)–(**f**) SBN crystals. Those experiments were done using a fluence of 15 J/cm^2.

observed with SBN. The underlying question is why this happens, given that the two samples have almost the same absorption at 532 nm. At this wavelength, both samples show a resonant $^2G_{9/2}$ and $^4G_{7/2}$ to ground state ($^4I_{9/2}$) transition (see Fig. 5, absorption spectra of BNN and SBN).[42] If this absorption explains the intense emission of Nd in BNN, the same situation should be shown for the SBN sample.

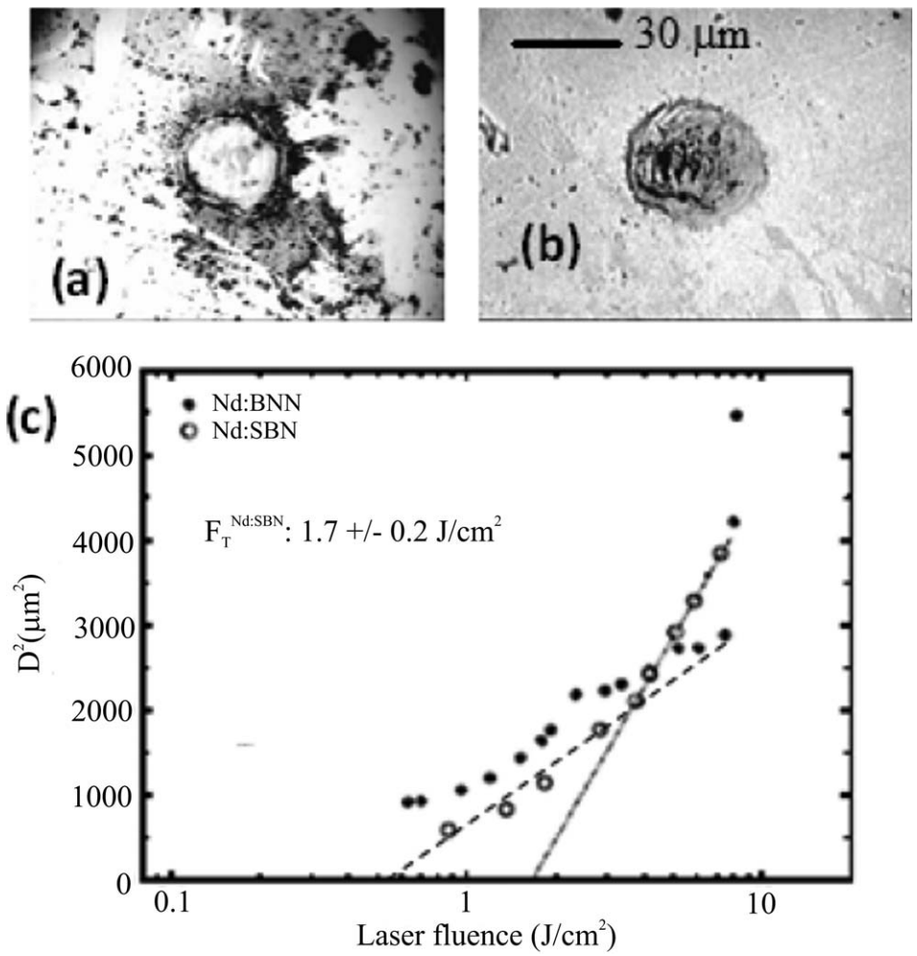

FIG. 3. (**a**) SBN and (**b**) BNN corresponding to optical microscopy pictures of the ablation holes. The scale is the same for (**a**) and (**b**). (**c**) D^2 as function of the ablation fluence at 355 nm for both crystals. BNN (full circles) and SBN (open circles). The data were fitted (dashed lines) to determine the ablation threshold.

We propose that this is a clear example of the so-called matrix effect from which the LIBS technique suffers. The only difference between SBN and BNN is the matrix from which the Nd ions and atoms are extracted. All the rest of the experimental parameters were carefully controlled in such a way as to ensure compatibility between the experiments; in spite of this, the Nd ion shows a greater emission in BNN than in the SBN sample.

So for the case of BNN, we believe that this effect can be exploited. We think that Nd ions can play a paramount role in assisting the ablation process at 532 nm. This means that, due to the absorption of the sample at this wavelength, the ablation process could be carried out with higher efficiencies than those where there is no absorption (i.e., $\lambda = 1064$ nm).

Plasma parameters determination. Several plasma parameters can be estimated from LIBS spectra, i.e., plasma temperature (t_k) and electron density (n_e), among others. Here, t_k and n_e are measured by employing the well-known methods of the Boltzmann plot and Stark broadening, respectively, which are described elsewhere.[39,43] The spectral transitions used to calculate these parameters were Ba emission located at 553.50, 577.80, 606.30, 634.17, 659.50, 705.99, 712.03, and 728.03 nm for temperature estimation, and Ba II 614.5 nm for n_e estimation.[44] The lines were selected according to (i) the availability of the spectroscopic parameter required and (ii) the emission lines observed in our experimental conditions. The temperature and electronic density for BNN and SBN crystals were calculated from data shown in Fig. 2.

Table I summarizes the electronic temperature and density values obtained in our experiments. After a preliminary inspection, we can say that electronic temperature and electronic density are strongly dependent on the excitation wavelength for both samples used in our experiments. When the BNN samples are excited at 532 nm, the temperature is two times greater than at excitation wavelengths of 1064 or 355 nm. In the case of SBN, the electronic temperature excited at 355 nm is three times higher than excitation at 1064 nm. On the other hand, for SBN, the electronic density, as shown in Table I, is three orders of magnitude greater for 355 nm excitation than for 1064 nm. The situation is different in the case of BNN, where the relation for the electronic density in the plasma at 1064 nm is 7 times lower than at 355 nm excitation.

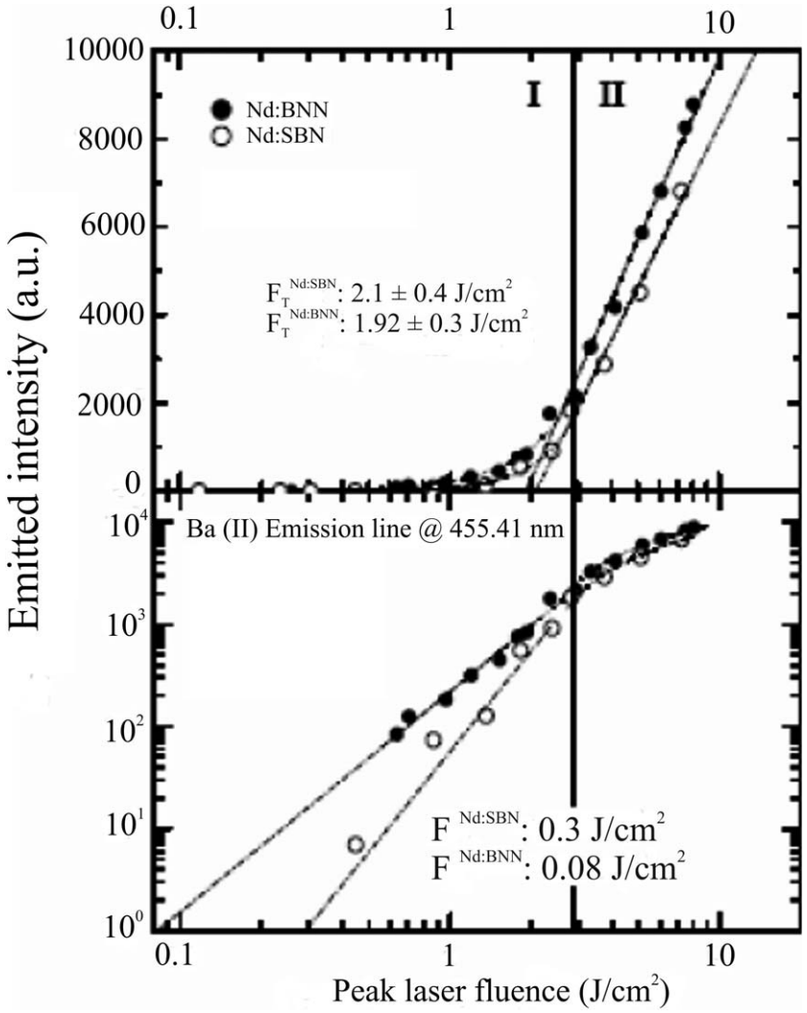

FIG. 4. Emission intensity (Ba II, 455.41 nm) versus ablation fluence at 355 nm excitation wavelength. The full circles correspond to BNN data while open circles correspond to the SBN. The bottom figure corresponds to the same set of data represented in log-log scale.

The absorption spectra of the samples are used to explain the abnormally high values of electronic temperature found in our experiments when excitation is carried out with different wavelengths (see Fig. 5). Both samples show an absorption edge at 355 nm, but it is clearly higher for SBN. Due to the location of the absorption edge, the crystal ionization at this wavelength can be reached by one photon absorption, and consequently, the ablation efficiency result is higher at 355 nm for the SBN crystal. This fact supports the higher temperature and electron density found in this material. The absorption spectra shown in Fig. 5 can also be used to explain an apparent contradiction in the values of
?1 electronic density for BNN and SBN at 532 and 355 nm. At 532 nm, the electronic density is nearly the same for both samples. This fact is shown in Fig. 5. By other way, the absorption at 355 nm is several times greater in BNN than SBN, which means that the absorption for SBN does not justify an increase in the electronic temperature of this sample.

Finally, in order to discuss the matrix effect commented upon in the previous section, we studied the assisted ablation by means of the Nd impurities present in the active crystals. Thus, we also analyzed the plasma data and then calculated the temperature and the electron density for the plasma obtained after excitation using a 532 nm laser wavelength. The values obtained for temperature [K] were: 29 100 and 30 000 for the BNN and SBN, respectively, while for the electronic density [cm^{-3}], the values were 6.2×10^{19} and 1.5×10^{19} for BNN and SBN, respectively. As can be seen, the values obtained for the temperature and the electronic density are higher at 532 nm than at 1064 nm. This fact could be tentatively explained taking into account that the Nd^{3+} ions, as impurities inside the crystals, play an important role in the plasma formation by assisting the ablation process by means of the impurity absorption by two-photon absorption for 532 nm excitation, resulting in ionization. Therefore, the presence of dopants in the active crystals could be an important sensitizer helping to perform in a controlled way the ablation process involved in the laser processing active crystals. The use of selective ablation by tuning the ablation laser source could be an interesting tool to achieve suitable performance for laser processing materials.

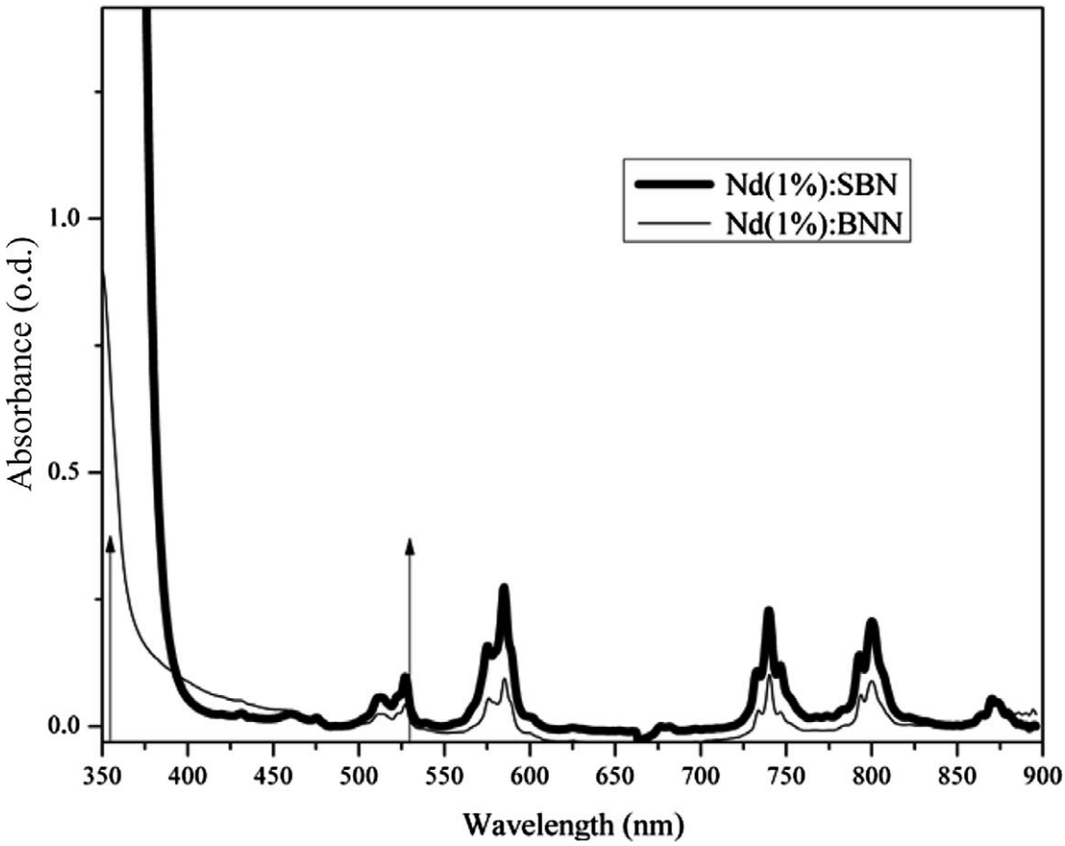

FIG. 5. Optical absorption spectra at room temperature. SBN and BNN are represented by solid and dashed line respectively. Arrows indicate the ablation wavelengths used in the experiments.

Conclusions

We have presented the ablation properties of active crystals (Nd-doped SBN and BNN) by using LIBS. Two different ablation regimes were identified by using this method. In this sense, by extrapolating to zero intensity, the straight line corresponding to regime II, the ablation threshold has been estimated for each sample. The values measured were 2.1 J/cm^2, which corresponds to the ablation threshold of the Nd : SBN sample, and 1.90 J/cm^2, which corresponds to Nd : BNN sample. By contrast, once the ablation rate changed (regime I), the extrapolation of the experimental points showed values of 0.3 and 0.08 J/cm^2 for the Nd : SBN and Nd : BNN crystals, respectively. These values could be understood as the higher limit of the damage threshold of each sample. By comparing the intensity versus fluence curve corresponding to Nd : SBN with the D^2 versus fluence, it is observed that the values measured for both techniques show a good agreement.

On the other hand, we calculated plasma parameters such as temperature and electron density from LIBS data. From these results, we conclude that the energy gap for the active crystal plays an important role in describing the plasma formation when the ablation wavelength is tuned with an absorption edge. Also, in this paper, we have introduced assisted ablation by means of the absorption by the Nd^{3+} impurities present in the crystals. Finally, we would like to remark that the selective assisted ablation of the active impurities inside the crystals could be an interesting feature that can optimize laser processing for photonics or technological applications, and we will explore this in future works.

TABLE I. Electronic temperature and electronic density for the BNN and SBN excited at 1064, 532, and 355 nm. Experiments were done using a fluence of 15 J/cm^2.

	Temperature (K)		$n_e \times 1 \times 10^{18}$ (cm^{-3})	
λ (nm)	BNN	SBN	BNN	SBN
1064	16 480 ± 1500	11 833 ± 1025	2.2 ± 0.2	0.5 ± 0.05
532	29 100 ± 2600	30 000 ± 2400	62 ± 5	15 ± 3
355	17 000 ± 1500	36 000 ± 2700	15 ± 2	140 ± 25

ACKNOWLEDGMENTS

This work was partially supported by PICT 2010-2575 and PIP 5990. The authors wish to thank Daniel Jaque for providing the samples for this work. FCA and GAT are researchers from CONICET.

1. C. Pasquini, J. Cortez, L.M.C. Silva, F.B. Gonzaga. "Laser Induced Breakdown Spectroscopy". J. Braz. Chem. Soc. 2007. 18(3): 463-512.
2. C.C. Garcia, H. Lindner, A. von Bohlen, C. Vadla, K. Niemax. "Elemental Fractionation and Stoichiometric Sampling in Femtosecond Laser Ablation". J. Anal. At. Spectrom. 2008. 23(4): 470-478.
3. J.B. Sirven, B. Sallé, P. Mauchien, J.L. Lacour, S. Maurice, G. Manhès. "Feasibility Study of Rock Identification at the Surface of Mars by Remote Laser-Induced Breakdown Spectroscopy and

Three Chemometric Methods". J. Anal. At. Spectrom. 2007. 22(12): 1471-1480.
4. K. Song, Y.I. Lee, J. Sneddon. "Recent Developments in Instrumentation for Laser Induced Breakdown Spectroscopy". Appl. Spectrosc. Rev. 2002. 37(1): 89-117.
5. F.C. Alvira, D.J.O. Orzi, G.M. Bilmes. "Surface Treatment Analyses of Car Bearings by Using Laser-Induced Breakdown Spectroscopy". Appl. Spectrosc. 2009. 63(2): 192-198.
6. T. Flores, L. Ponce, G. Bilmes, A. Arronte, F. Alvira. "Laser Induced Breakdown Spectroscopy of Prickly Pear's Spines and Glochids: A Qualitative Analysis". AIP Conf. Proc. 2008. 992(1): 1274-1279.
7. F.C. Alvira, F.R. Rozzi, G.M. Bilmes. "Laser-Induced Breakdown Spectroscopy Microanalysis of Trace Elements in Homo Sapiens Teeth". Appl. Spectrosc. 2010. 64(3): 313-319.
8. F.C. Alvira, L. Ponce, M. Arronte, G.M. Bilmes. "Time Resolving Imaging Spectroscopy Applied to the Analysis of Plasmas Generated by Pulsed Lasers". J. Phys.: Conf. Ser. 2011. 274(1): 012085.
9. W.B. Lee, J. Wu, Y.I. Lee, J. Sneddon. "Recent Applications of Laser-Induced Breakdown Spectrometry: A Review of Material Approaches". Appl. Spectrosc. Rev. 2004. 39(1): 27-97.
10. F.J. Gordillo-Vázquez, A. Perea, A.P. McKiernan, C.N. Afonso. "Electronic Temperature and Density of the Plasma Produced by Nanosecond Ultraviolet Laser Ablation of LiF". Appl. Phys. Lett. 2005. 86(18): 1-3.
11. L. Xu, V. Bulatov, I. Schechter. "Spectroscopic Imaging of Laser-Induced Plasma". Anal. Chem. 1996. 68(17): 2966-2973.
12. D.B. Geohegan. "Fast Intensified-CCD Photography of YBa2Cu3O7-x Laser Ablation in Vacuum and Ambient Oxygen". Appl. Phys. Lett. 1992. 60(22): 2732-2734.
13. A. Mitra, R.K. Thareja. "Determination of Laser Ablation Threshold of Teflon at Different Harmonics of Nd : YAG Laser Using Photothermal Deflection Technique". J. Mater. Sci. 1999. 34(3): 615-619.
14. J.A. Sell, D.M. Heffelfinger, P. Ventzek, R.M. Gilgenbach. "Laser Beam Deflection as a Probe of Laser Ablation of Materials". Appl. Phys. Lett. 1989. 55(23): 2435-2437.
15. J.A. Sell, D.M. Heffelfinger, P.L.G. Ventzek, R.M. Gilgenbach. "Photoacoustic and Photothermal Beam Deflection as a Probe of Laser Ablation of Materials". J. Appl. Phys. 1991. 69(3): 1330-1336.
16. M. Hashida, A.F. Semerok, O. Gobert, G. Petite, Y. Izawa, J.F. Wagner. "Ablation Threshold Dependence on Pulse Duration for Copper". Appl. Surf. Sci. 2002. 197-198: 862-867.
17. S.H. Ko, Y. Choi, D.J. Hwang, C.P. Grigoropoulos, J. Chung, D. Poulikakos. "Nanosecond Laser Ablation of Gold Nanoparticle Films". Appl. Phys. Lett. 2006. 89: 141126.
18. S. Lazare, V. Granier. "Excimer Laser Light Induced Ablation and Reactions at Polymer Surfaces as Measured with a Quartz-Crystal Microbalance". J. Appl. Phys. 1988. 63(6): 2110-2115.
19. Y. Domankevitz, N.S. Nishioka. "Measurement of Laser Ablation Threshold with a High-Speed Framing Camera". IEEE J. Quantum Electron. 1990. 26(12): 2276-2278.
20. D. Vouagner, C. Beleznai, J.P. Girardeau-Montaut, C. Templier, H. Gonnord. "A New Method to Determine Laser Damage Threshold for Thin Diamond-Like Carbon Films on Silicon". Diamond Relat. Mater. 2000. 9(3-6): 786-791.
21. G.M. Bilmes, D.J.O. Orzi, O.E. Martínez, A. Lencina. "A Real Time Method for Surface Cleanliness Measurement". Appl. Phys B: Lasers Opt. 2006. 82(4): 643-648.
22. D.O. Orzi, F.C. Alvira, G.M. Bilmes. "Determination of Femtosecond Ablation Thresholds by Using Laser Ablation Induced Photoacoustics (LAIP)". Appl. Phys. A. 2013. 110(3): 735-739.
23. D.J.O. Orzi, G.M. Bilmes. "Identification and Measurement of Dirt Composition of Manufactured Steel Plates Using Laser-Induced Breakdown Spectroscopy". Appl. Spectrosc. 2004. 58(12): 1475-1480.
24. N. Carmona, M. Oujja, E. Rebollar, H. Römich, M. Castillejo. "Analysis of Corroded Glasses by Laser Induced Breakdown Spectroscopy". Spectrochim. Acta, Part B. 2005. 60(7-8): 1155-1162.
25. B. Wu, P.L. Chu, H. Hu, Z. Xiong. "UV-Induced Surface-Relief Gratings on $Linbo_3$ Channel Waveguides". IEEE J. Quantum Electron. 1999. 35(10): 1369-1373.
26. K. Chen, J. Ihlemann, P. Simon, I. Baumann, W. Sohler. "Generation of Submicron Surface Gratings on $LiNbO_3$ by Ultrashort UV Laser Pulses". Appl. Phys. A: Mater. Sci. Process. 1997. 65(4-5): 517-518.
27. X. Zeng, X.L. Mao, R. Greif, R.E. Russo. "Experimental Investigation of Ablation Efficiency and Plasma Expansion During Femtosecond and Nanosecond Laser Ablation of Silicon". Appl. Phys. A: Mater. Sci. Process. 2005. 80(2): 237-241.
28. B. Tan. "Deep Micro Hole Drilling in a Silicon Substrate Using Multi-Bursts of Nanosecond UV Laser Pulses". J. Micromech. Microeng. 2006. 16(1): 109-112.
29. D. Wortmann, J. Gottmann. "Fs-Laser Structuring of Ridge Waveguides". Appl. Phys. A: Mater. Sci. Process. 2008. 93(1): 197-201.
30. P. Molina, M. de la O. Ramírez, L.E. Bausá. "Strontium Barium Niobate as a Multifunctional Two-Dimensional Nonlinear "Photonic Glass". Adv. Funct. Mater. 2008. 18(5): 709-715.
31. J.W. Fleischer, M. Segev, N.K. Efremidis, D.N. Christodoulides. "Observation of Two-Dimensional Discrete Solitons in Optically Induced Nonlinear Photonic Lattices". Nature. 2003. 422(6928): 147-150.
32. J. Lamela, G.L.A. Ródenas, G. Lifante, D. Jaque, F. Jaque, A.A. Kaminskii. "Effects of Laser Light Confinement in Periodically Poled Orthorhombic Non-Centrosymmetric $Ba_2NaNb_5O_{15}$ Crystals". Laser Phys. Lett. 2008. 5(4): 291-295.
33. G. Della Valle, R. Osellame, N. Chiodo, S. Taccheo, G. Cerullo, P. Laporta, A. Killi, U. Morgner, M. Lederer, D. Kopf. "C-Band Waveguide Amplifier Produced by Femtosecond Laser Writing". Opt. Express. 2005. 13(16): 5976-5982.
34. G.A. Torchia, A. Rodenas, A. Benayas, E. Cantelar, L. Roso, D. Jaque. "Highly Efficient Laser Action in Femtosecond-Written Nd : Yttrium Aluminum Garnet Ceramic Waveguides". Appl. Phys. Lett. 2008. 92(11): 111103.
35. S. Nolte, M. Will, J. Burghoff, A. Tuennermann. "Femtosecond Waveguide Writing: A New Avenue to Three-Dimensional Integrated Optics". Appl. Phys. A: Mater. Sci. Process. 2003. 77(1): 109-111.
36. A. Ródenas, D. Jaque, G.A. Torchia, C. Mendez, I. Arias, L. Roso, P. Moreno, F. Agulló-Rueda. "Femtosecond Laser Induced Micromodifications In Nd : SBN Crystals: Amorphization and Luminescence Inhibition". J. Appl. Phys. 2006. 100: 113517.
37. J. Lamela, A. Rodenas, D. Jaque, F. Jaque, G.A. Torchia, C. Mendez, L. Roso. "Field Optical and Micro-Luminescence Investigations of Femtosecond Laser Micro-Structured Nd : YAG Crystals". Opt. Express. 2007. 15(6): 3285-3290.
38. M.O. Ramírez, D. Jaque, L.E. Bausá, J. García Solé, A.A. Kaminskii. "Coherent Light Generation from a Nd : SBN Nonlinear Laser Crystal Through its Ferroelectric Phase Transition". Phys. Rev. Lett. 2005. 95(26): 267401.
39. D.A. Cremers, L.J. Radziemski. Handbook of Laser-Induced Breakdown Spectroscopy. Chichester, UK: John Wiley and Sons, 2006.
40. A.W. Miziolek, V. Palleschi, I. Schechter, editors. Laser-Induced Breakdown Spectroscopy. Cambridge, UK: Cambridge University Press, 2006.
41. J.P. Singh, S.N. Thakur, editors. Laser-Induced Breakdown Spectroscopy. Amsterdam, Netherlands: Elsevier, 2007. 1st ed.
42. W. Koechner. Solid-State Laser Engineering. Berlin, Germany: Springer, 1999. 5th rev. and updated ed.
43. L.J. Radziemski, D.A. Cremers, editors. Laser-Induced Plasmas and Applications. New York, USA: Taylor and Francis, 1989.
44. NIST. "Atomic Spectra Database". http://physics.nist.gov/PhysRefData/ASD/ [accessed Oct 31 2013].

Queries for apls-68-04-13

1. SBN was written here twice. I changed it to "BNN and SBN". Change OK? Editor